Nanoscale

Accepted Manuscript

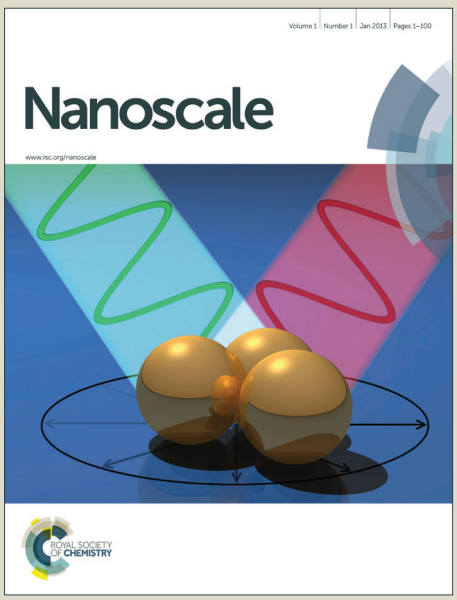

ROYAL SOCIETY OF CHEMISTRY

www.rsc.org/nanoscale

Nanoscale

RSC Publishing

ARTICLE

7,7,8,8-tetracyanoquinodimethane-assisted one-step electrochemical exfoliation of graphite and its performance as an electrode material

Cite this: DOI: 10.1039/x0xx00000x

Received 00th XXX XXX,
Accepted 00th XXX,XXX

DOI: 10.1039/x0xx00000x

www.rsc.org/

Partha Khanra,[a] Chang-No Lee,[a] Tapas Kuila,[b] Nam Hoon Kim,[a*] Min Jun Park,[a] Joong Hee Lee,[a,c]*

A green approach for the preparation of water-dispersible functionalized graphene via one-step electrochemical exfoliation of graphite using 7,7,8,8-tetracyanoquinodimethane (TCNQ) anions as surface modifiers and electrolytes was described. TCNQ is an organic charge-transfer complex with electron acceptors and noble electrical properties. The exfoliation of graphite to a few-layer graphene sheets was confirmed by transmission electron microscopy (TEM) and atomic force microscopy (AFM) image analysis. Chemical state, surface functional groups and chemical compositions of bulk graphite as well as TCNQ-functionalized graphene sheets were investigated by Fourier-transformed infrared (FT-IR) and X-ray photoelectron spectroscopy (XPS) analysis. Adsorption of TCNQ on the surface of graphene sheets was confirmed by the appearance of N1s peak at ~399.4 eV in the XPS of TCNQ-functionalized graphene. Exfoliation of bulk graphite to functionalized graphene sheets was further confirmed by the appearance of a sharp single peak at ~2695 cm^{-1} along with increased intensity ratios of the D-band to the G-band. Electrochemical performance of TCNQ-functionalized graphene sheet was investigated using 1 M Na_2SO_4 and 1 M KOH aqueous solution. Cyclic voltammetry (CV) and galvanometric charge-discharge experiments revealed that TCNQ-functionalized graphene could be used as a supercapacitor electrode material. The specific capacitance values of TCNQ-modified graphene measured with electrolytes (1 M KOH and 1 M Na_2SO_4) were 324 and 140 F g^{-1}, respectively, at a current density of 1 A g^{-1}. Impedance spectroscopic analysis revealed that the charge transfer process was dependent on surface functionalization and interaction between the electrode and electrolyte.

1. Introduction

Graphene is the thinnest layer of graphite, and consists of close-packed hexagonal lattices of carbon atoms linked by sp^2 bonds and mobile π-electrons above and below the two-dimensional sheets. Its unique structure endows graphene with very high electrical conductivity, chemical resistivity, electrochemical stability, optical properties, charge-carrier mobility, large specific surface area, thermal conductivity, exceptional mechanical flexibility, and good bio-compatibilitylity.[1-6] Therefore, graphene has attracted significant attention during recent years in the areas of microelectronics, sensors, and energy storage devices. Among these areas, research into new energy materials has gained significant attention due to the concern regarding limited fossil fuel reserves. The mostly used energy resources, such as mineral oil, coal, and nuclear fuel, cannot be recovered after consumption. Therefore, the storage of limited energy resources has gained a worldwide attention. Ongoing studies on energy storage materials have shown that supercapacitor devices can provide portable energy sources and advanced energy storage solutions for applications in smart grids, biomass, urban lifestyle devices, and consumer care industries.[7-9] Supercapacitors or ultracapacitors can store electrical energy by electrical double layer capacitance (EDLC) through an electrostatic charge storage mechanism and pseudocapacitance via Faradic reactions.[7-9] Total specific capacitance of an electrode material is improved significantly by the contribution of pseudocapacitance, which is controlled by surface functional groups, electrical conductivity and the interaction with the electrolyte. In aqueous electrolyte, hydrophilicity of graphene is the key factor to improve the capacitance performance. However, the hydrophilicity of pristine graphene is very poor, which limits its applications as an energy storage electrode material.[7-9] To overcome this shortcoming, the surface of graphene has been functionalized using small organic molecules or macromolecules. Surface modified graphene has been used extensively in the fabrication

of polymers, composites, field effect transistors, dye-sensitized solar cells, biosensors, and supercapacitor devices.[10-15] The hydrophilicity of pristine graphene can also be improved by doping the skeleton of graphene with heteroatoms (N, S, O). Surface-modified graphene or heteroatom-doped graphene can serve as a multifunctional podium to enhance supercapacitor device performance.

Several methods have been developed to obtain surface modified graphene. The most commonly used method involves chemical oxidation of graphite, conversion of multilayer graphite oxide to monolayer graphene oxide (GO), and surface modification of the GO followed by reduction of the surface modified GO. Indeed, this is the cheapest and easiest route to obtain chemically functionalized graphene. Moreover, the properties of graphene can be easily tuned by chemical grafting of different kinds of functional groups onto the surface of graphene. However, several hazardous and toxic chemicals are used in this approach. Moreover, chemically derived graphene contains huge surface defects due to the destructive oxidation process. Reduction of GO or surface modified GO cannot restore the full π-electronic conjugated network and thus, surface modified graphene generally suffers from low electrical conductivity and loss of some other unique features of graphene. To address this issue, sono-chemical preparation of surface modified graphene was introduced. This method is green and does not require a destructive oxidation process. However, the yield from sono-chemical preparation is very low.[16] Surface modification of graphene grown by chemical vapor deposition (CVD) is very difficult from a practical chemistry point of view. Therefore, a cost-effective, time saving, and eco-friendly route for the production of surface modified graphene is needed.

Liu et al. first reported a one-step electrochemical route to exfoliate graphite in presence of an ionic liquid/water mixture.[17] In this process, the edge planes of graphite are oxidized due to the electrolysis in presence of ionic liquid/water mixture. In addition, exfoliation of graphite occurred due to the intercalation of ionic liquids in between the graphitic layers. In a similar method, Wang et al. synthesized a few-layer graphene sheets in propylene carbonate (PC) electrolyte and lithium salt.[18] The Li/PC complex are intercalated in the graphitic layers of the negative electrode. An interlayer stress was generated at the grain boundary of graphite layers due to the decomposition of electrolyte at high voltage. However, the dispersion of exfoliated graphene sheets are limited in organic solvents as described by Liu et al. and Wang et al.[17,18] Moreover, graphitic nanoplatelets were formed while taking ionic liquid/water mixture as the electrolyte.[17] In contrast, monolayer graphene synthesis directly from graphite has been demonstrated using an aqueous solution of 7,7,8,8-tetracyanoquinodimethane (TCNQ) as an electrolyte. The current method shows that the degree of exfoliation of graphite can be controlled by the concentration of TCNQ anion in the electrolyte solution. The electrochemically exfoliated functionalized graphene sheets are highly dispersible in water and can be used as potential material for the development of high performance energy storage electrode for supercapacitor devices. In addition, the process is eco-friendly and produces graphene with a few defects. Moreover, it is profitable due to the rapidity of the process and consumption of very low amounts of electricity compared to other methods such as CVD, plasma-enhanced CVD, chemical oxidation-reduction of graphite, and sono-chemical approaches. We characterized the morphology and structure of the electrochemically exfoliated materials to confirm the formation of graphene from graphite. Electrochemical performance was evaluated by cyclic voltammetry (CV), charge-discharge analysis, and electrochemical impedance spectroscopy (EIS) analysis.

2. Experimental

2.1 Materials

High-purity graphite rods were purchased from Qingdao Xinlei Graphite Produce Co., Ltd., China. TCNQ and dimethyl sulfoxide (DMSO) were purchased from TCI, Japan. Potassium hydroxide and sodium sulfate were purchased from Samchun Pure Chemical Co. Ltd., Korea.

2.2 Electrochemical exfoliation of graphite

Graphite rods were used as the source of graphene. Pretreatment of TCNQ is an essential step to dissolve it in water. In a typical process, 25 and 100 mg TCNQ were mixed with 0.25 and 1 ml DMSO, respectively and kept at room temperature for 12 h. This solution was then dried under vacuum at 80° C for 6 h. The resulting solid powder was re-dispersed in 0.01 M KOH solution to obtain a solution of TCNQ anions.[19] This solution was mixed with 100 ml DI water and the resulting mixture was used as the electrolyte. A constant voltage from a DC (25 V) power supply was applied between two graphite electrodes for 12 h. Black dispersion was filtered through a PTFE membrane (pore size ~0.2 μm) and washed with de-ionised (DI) water until the pH of the filtrate reached to ~7. The obtained product was dispersed in DI water and centrifuged at 3000 r.p.m. for 15 min to remove large graphite particles. The upper stable solution was collected for further characterization. The obtained products were designated TCNQG1 (25 mg TCNQ) and TCNQG2 (100 mg TCNQ), respectively.

2.3 Characterization

Fourier transform infrared spectroscopy (FT-IR) was performed using a Nicolet 6700 spectrometer (Thermo Scientific, USA) over the wave number range of 4000-400 cm^{-1}. Raman spectra of pure graphite, TCNQG1, and TCNQG2 were obtained on a Nanofinder 30 (Tokyo Instruments Co., Japan). The chemical characteristics of graphite, TCNQG1, and TCNQG2 were analyzed by AXIS-NOVA X-ray photoelectron spectroscopy (XPS) (Kratos Analytical Ltd, UK) using 160 eV of pass energy and a step size of 0.7 eV to ensure the purity and cleanliness of the samples. Pass energy of 50 eV and a step size of 0.1 eV were used for narrow spectra, and the energy resolution was < 0.6 eV, which was determined as the full-width-at-half-maximum (FWHM) of the Au $4f_{7/2}$ line calibrated

at 83.9 eV. Atomic force microscopy (AFM) analysis of TCNQG1 and TCNQG2 was carried out using the XE-100 atomic force microscope (PARK systems, Korea). AFM samples were prepared by deposition of a water dispersion of functionalized graphene on the surface of a silicon substrate followed by drying in a N_2 atmosphere. Microstructures of the samples were investigated using a JEM-2200 FS transmission electron microscope (TEM) (JEOL, Japan). Uniform aqueous dispersion of functionalized graphene was drop-casted on a fresh lacey carbon Cu-grid. Thermogravimetric analysis (TGA) was carried out on a Q50 TGA (TA Instruments, USA) at a heating rate of 5°C min^{-1} from 60-800 °C in nitrogen atmosphere.

2.4 Electrochemical measurements

Electrochemical performance was evaluated using a CH660D electrochemical workstation (CH Instrument, USA) and three electrode systems at ambient temperature (~24 °C). The working electrode was prepared by the deposition of functionalized graphene mixed with 5 wt.% PVDF on a nickel foam electrode. Mass loading on each electrode was 3 mg cm^{-2}. Prior to electrode preparation, the nickel foam was cleaned via sonication for 20 min and dipped in a 5% aqueous HCl solution followed by washing with DI water. Finally, the nickel foam was sonicated in acetone for 20 min. It was then dried in a nitrogen atmosphere and kept inside a desiccator before drop-casting of TCNQ-functionalized graphene. Electrochemical performance was evaluated by CV, galvanometric charge-discharge, and EIS. 1 M Na_2SO_4 and 1 M KOH aqueous solutions were used as electrolytes. The reference electrode and counter electrode were AgCl/Ag and platinum, respectively. CV was carried out at scan rates from 5 to 200 mV in the potential range of -1.0~0.0 V. EIS measurements were carried out with circuit potential in the frequency range of 0.01 to 105 Hz. Capacitance values were calculated from galvanometric charge-discharge curves.

3. Results and discussion

3.1 Mechanism of electrochemical exfoliation

Electrochemical exfoliation of graphite occurred in the presence of an aqueous solution of TCNQ anion radicals, resulting in the generation of water-dispersible graphene. The schematic diagram of electrochemical exfoliation mechanism is shown in Fig. S1. Radical anions of TCNQ are of considerable interest due to their electrical conductivity and high solubility in water. TCNQ comprises an abundant π-electron cloud that can be delocalized with the π-electronic conjugation of graphene, thereby improving the electrical conductivity of hybrid materials. TCNQ anions interact strongly with π-electron-rich graphene surfaces, and the functionalized graphene is easily dispersed in water. However, untreated TCNQ would not be used directly as an electrolyte because of its limited solubility in water.[19,20]

Electrochemical exfoliation of graphite occurs due to swelling of the electrode, which is similar to what has been observed for ionic liquids and poly (sodium-4-styrenesulfonate).[17] However, the exact mechanism underlying the exfoliation of graphite is still unclear. Electrochemical exfoliation of graphite can occur in either alkaline or acid medium and the exfoliated graphene can be modified simultaneously with functional groups present in the electrolyte. We hypothesize that TCNQ anions attached to the surface of graphite anode via electrostatic interactions under an applied voltage. Subsequently, graphite layers along with TCNQ-anions separated from the anode under electrical potential and swelled in the aqueous solution. Free TCNQ-anions were again adsorbed on the surface of the anode, and this process was repeated for a long time. In contrast, the weight of the cathode remained unchanged throughout the process. TCNQ anions likely interact with the surface of graphene by π-π interactions.

3.2 Morphological observation.

TEM, high resolution TEM (HR-TEM), and selected area electron diffraction (SAED) pattern images of TCNQG1 and TCNQG2 are shown in Fig. 1(a-d). TCNQG1 sheets were transparent and folded in several regions, indicating the flexible nature of graphene sheets. Ferrari et al. report that HR-TEM is very helpful to identify the number of layers at different locations by looking the number of lattice fringes visible on the edges of the folded graphene sheets, since the electron beam is locally parallel to the graphene sheet at the folded region.[21] The HR-TEM images of TCNQG1 and TCNQG2 indicate the formation of a few-layer graphene due to the appearance of several lattice fringes parallel to each other. The number of layers in a graphene sheet can also derived by the analysis of SAED pattern of the freely suspended sheets for varying incidence angles. It is believed that the intensities of {1100} and {0110} diffraction spots for monolayer graphene are significantly higher than those of the {2110} and {1120} spots.[21,22,23] However, it is very difficult to clearly distinguish the intensity of the diffraction spots for TCNQG1 and TCNQG2 (shown in the inset of Fig. 1b and 1d), since the SAED pattern consists of several unresolved spots.[24] It may be attributed to the non-covalent adsorption of TCNQ anions on the surface of exfoliated graphene sheets as well as the presence of oxygen functional groups formed during the electrochemical exfoliation of graphite.[25,26] However, the physical adsorption of un-reacted TCNQ on the surface of graphene sheets cannot be ruled out. Yase et al. show that TCNQ-TTF (2,2-bis-1,3-dithiole) complex can exhibit typical diffraction pattern which is very close to the diffraction pattern of crystalline materials.[27] Thus, it is expected that the unresolved diffraction spots in the TCNQG1 and TCNQG2 are attributed to the presence of TCNQ on the surface of functionalized graphene sheets. Interestingly, the diffraction pattern of TCNQG2 is markedly different with that of TCNQG1 due to the loss of long range ordering of graphite and higher content of surface adsorbed TCNQ.[26,27] These observations are in good agreement with the observation of Chen et al. for amino acid-reduced graphene oxide.[26] The TEM, HR-TEM images and SAED pattern indicated the formation of few-layers functionalized graphene

sheets.[26,28] The thicknesses of the functionalized graphene sheets (TCNQG1 and TCNQG2) were analyzed by AFM imaging of samples coated on the surface of a silicon substrate. AFM images of TCNQG1 and TCNQG2 are shown in Fig. 2(a,b). The average thickness of TCNQG1 was ~2.4 nm. In contrast, the average thickness of TCNQG2 was ~1.0 nm, indicating better exfoliation of graphite in the latter sample due to a higher concentration of TCNQ. This observation is in good agreement with the SAED patterns of TCNQG1 and TCNQG2.

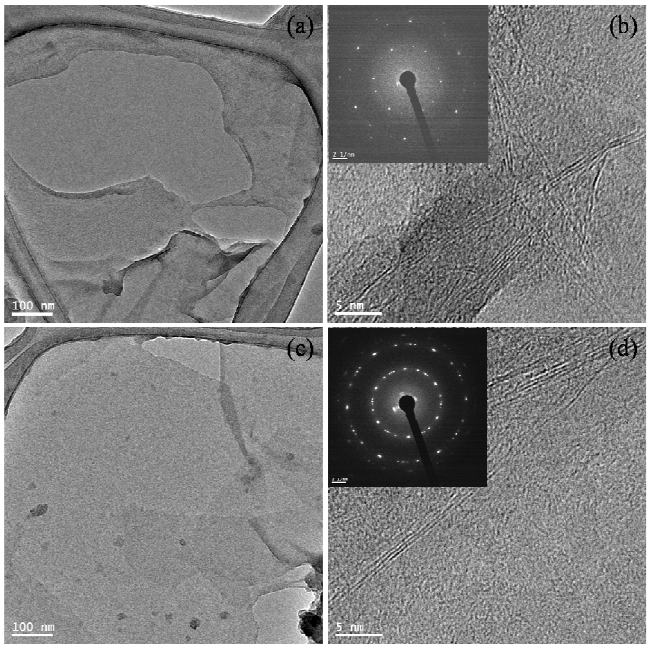

Fig. 1 (a,c) TEM and (b,d) HR-TEM images of (a,b) TCNQG1 and (c,d) TCNQG2. The insets in Fig. 1(b) and 1(d) show SAED pattern images of TCNQG1 and TCNQG2, respectively.

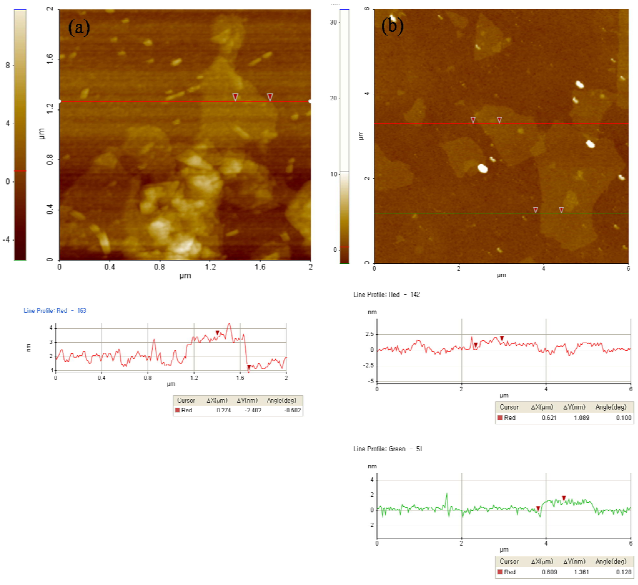

Fig. 2 AFM images of (a) TCNQG1 and (b) TCNQG2.

3.3 FT-IR spectra analysis

FTIR spectroscopy was carried out to investigate the surface chemical nature of pristine graphite and exfoliated graphene. FT-IR spectra of pristine graphene, TCNQG1, and TCNQG2 are shown in Fig. 3. The spectrum of pristine graphite had broad absorption bands at 3445 and 1030 cm^{-1} corresponding to O-H and C-O stretching vibrations, respectively. We ascribed the absorption peaks at 1565 and 1644 cm^{-1} of pristine graphite to the skeletal vibrations of C=C.[29] A few new peaks appeared after exfoliation of graphite, indicating changes in the surface properties of graphene due to the adsorption of TCNQ. In the case of TCNQG2 (Fig. 3), we assigned the intense peaks observed at 1580 and 1380 cm^{-1} to combinational skeletal vibrations of C=C bonds and C-H vibration bonds of TCNQ, respectively.[19] Moreover, the strong absorption peaks at 2920, 2845, and 1025 cm^{-1} for TCNQG2 correspond to the stretching vibrations of C-H and -CH_2- functional groups.[16,28] Interestingly, all the above-mentioned absorption peaks were present in TCNQG1 but at much lower intensities than observed for TCNQG2, suggesting better functionalization of the exfoliated materials at a higher concentration of TCNQ.

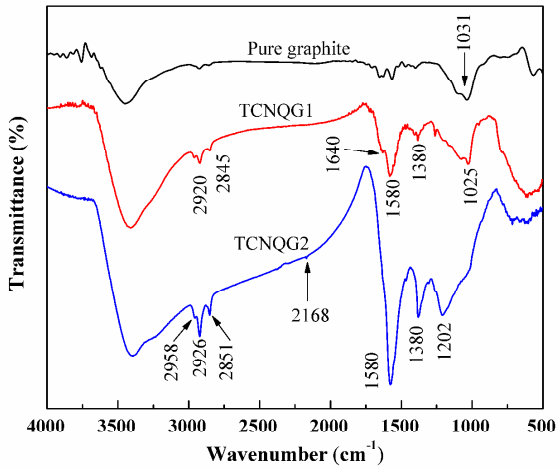

Fig. 3 FT-IR spectra of pure graphite, TCNQG1, and TCNQG2 showing the appearance of new peaks after exfoliation.

3.4 Raman spectra analysis

Raman spectroscopy is an essential tool to investigate the crystalline properties of graphene-based materials. Raman spectra of graphite, TCNQ1, and TCNQG2 are shown in Fig. 4. Raman spectra of graphitic materials were characterized by two main features: the G-band and D-band. The G-band is contributed by the double degenerated phonon mode (E_{2g}) at the centre of the benzoic ring due to the sp^2 network between the carbon atoms. Electron phonon coupling in graphene causes Kohn anomalies, which increase phonon dispersion. Generally, the G-band of graphitic materials is observed at ~1575 cm^{-1}.[30-32] In the present study, the G-band of TCNQG1 and TCNQG2 appeared at 1579 and 1582 cm^{-1}, respectively. The higher

wavelength of the G-band of functionalized graphene (TCNQG1 and TCNQG2) than that of bulk graphite indicated the presence of non-adiabatic Kohn anomalies due to the presence of electron acceptor TCNQ anions. The higher wavelength of the G-bands may also be due to the formation of oxygen functional groups in the electrochemically-exfoliated graphene during electrolysis in an alkaline medium. These observations were consistent with the FT-IR spectra analysis results, confirming the formation of oxygen functional groups in the TCNQ-functionalized graphene sheets. In addition, the G-band shifted to a higher wavelength as the concentration of TCNQ increased. The D-band originates from the breathing mode of the k-point of A_{1g} symmetry and is a measure of the degree of disorder of graphene.[30-32] The D-band of bulk graphite, TCNQG1, and TCNQG2 appeared at 1345, 1353, and 1348 cm^{-1}, respectively. The relative intensity of the D- to the G-band (I_D/I_G) is frequently used to determine the degree of disorder in a sp^2 network structure of graphene, desorption of hydrogen, thermal stability, and conversion of sp^3 and/or sp^2 bonds to sp^2 and/or sp^3 bonds.[32] Raman spectra analysis revealed that the I_D/I_G ratios for bulk graphite, TCNQG1, and TCNQG2 were 0.03, 1.02, and 1.04, respectively. The increase in I_D/I_G of the exfoliated samples indicated the adsorption of TCNQ-anion and the presence of other sp^3 defects due to electrolytic oxidation of graphene. The appearance of a single 2D-band in the Raman spectra of graphene was a direct evidence of graphene formation and very useful to determine the number of layers. The 2D-band of graphite appeared as a doublet band with one peak at 2682 cm^{-1} and the other at 2716 cm^{-1}. In contrast, the 2D-bands of TCNQG1 and TCNQG2 were sharp relative to that of bulk graphite with a single peak at ~2695 cm^{-1}. Based on the observations of Ferrari et al. and Wang et al., the Raman spectra of the functionalized graphene samples clearly indicated the formation of few-layer graphene.[33, 34] Interestingly, the intensity ratios of the 2D band to the G band (I_{2D}/I_G) increased with increasing concentration of surface-modifying agent in the electrolyte solution. The I_{2D}/I_G ratios were 0.09 and 0.13 for TCNQG1 and TCNQG2, respectively. All these observations suggest that more exfoliation of graphite occurred at the high concentration of TCNQ than at the low concentration of TCNQ.

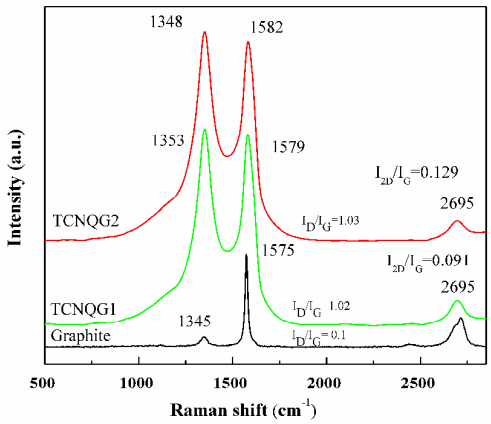

Fig. 4 Raman spectra of pure graphite, TCNQG1, and TCNQG2

3.5 XPS analysis

XPS was performed to investigate the presence of surface functional groups and to determine the chemical state and composition of the bulk graphite, TCNQG1, and TCNQG2 samples. XPS survey spectra clearly showed a change in chemical composition from bulk graphite to TCNQG1 to TCNQG2 (Fig. S2 in the supporting information). The intensity of the C1s peak (284 eV) decreased and that of the O_{1s} peak (532 eV) increased significantly in the survey spectra of TCNQG1 compared to those of bulk graphite. This is likely due to the electrochemical oxidation of exfoliated graphene sheets during the electrochemical exfoliation experiment. In contrast, the intensity of the C1s peak increased and that of the O1s peak decreased remarkably in the XPS survey of TCNQG2. It may be attributed to the KOH-induced removal of oxygen functional groups from the exfoliated graphene sheets. This observation is in good agreement with the observation of Fan et al. who studied the deoxygenation of graphene oxide using aqueous KOH solution.[35] In the case of TCNQG1, the concentration of KOH was very low and not sufficient for the removal of oxygen functional groups. Oxygen removal efficiency increased with increasing amounts of KOH in solution. In addition, a small N1s peak at 399.4 eV was observed for TCNQG2 due to the formation of a C-N bond between TCNQ anions and the graphene sheets. Deconvoluted XPS of bulk graphite are shown in Fig. S3 of supporting information. Peaks at 284.6, 286.6, and 289.8 eV corresponded to sp^2 carbons, C=O bonds, and π-π* interactions, respectively. Deconvoluted C1s and N1s spectra of functionalized graphene sheets (TCNQG1 and TCNQG2) are shown in Fig. 5(a-d). In the case of TCNQG1, the peaks located at 284.5, 286.1, 287.1 and 288.5 eV are correspond to the C-C/C=C, C-N, C-O, C-O-C, and C=O, respectively. Oxygen functional groups were formed by the electrochemical oxidation of exfoliated graphite sheets, as reported in a previous study.[36] The C1s spectrum of TCNQG2 was quite different from that of TCNQG1. The peak related to C-O-C at 287.1 eV was absent from the C1s spectrum of TCNQG2 (Fig. 5(c)). Moreover, the intensities of the C-O and C=O peaks also decreased. This may be due to KOH-induced removal of oxygen functional groups as described earlier. XPS-elemental analysis data shown in Table 1 also support these observations. The oxygen content of TCNQG2 was much lower than that of TCNQG1. N1s deconvoluted spectra clearly revealed the existence of nitrogen functional groups in the TCNQG1 sample (Fig. 5b) in the form of two peaks at 400.0 and 403.3 eV. According to Boyd et al., the peak at 403.3 eV is due to surface contamination and nitrogen entrapment from the atmosphere during deposition of the specimen on the substrate.[37] The appearance of a lower binding energy peak at 400.0 eV can be ascribed to the formation of NO radicals from the entrapped nitrogen. The N1s spectrum of TCNQG2 had an additional peak at 399.2 eV, indicating the formation of C-N bonds. These findings confirm that the concentration of TCNQ

plays an important role in the functionalization of electrochemically-prepared graphene sheets.[38]

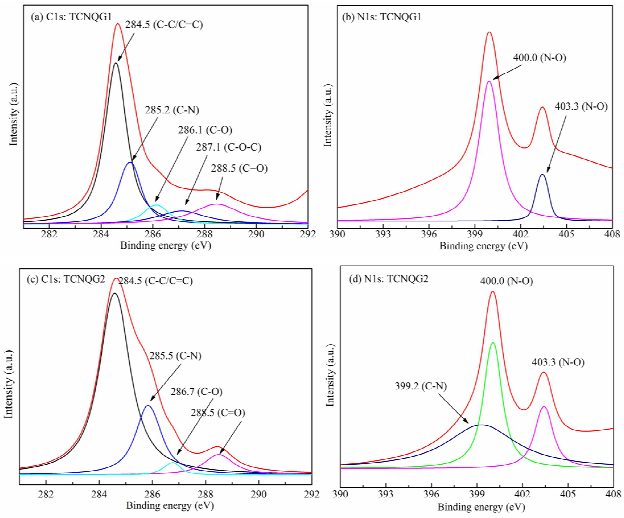

Fig. 5 (a) C1s XPS of TCNQG1, (b) N1s XPS of TCNQG1, (c) C1s XPS of TCNQG2 and (d) N1s of TCNQG2.

Table 1. Elemental composition of TCNQG1 and TCNQG2 derived from XPS elemental analysis

Sample	Carbon	Oxygen	Nitrogen	O/C
TCNQG1	77.42	20.62	1.96	0.27
TCNQG2	81.51	16.97	1.54	0.21

3.5 Thermogravimetric analysis

Thermogram (TG) and derivative thermogram (DTG) curves of pure graphite, TCNQG1, and TCNQG2 are shown in Fig. 6. Bulk graphite is thermally stable; only ~1.1% mass loss was observed at 800° C. In contrast, mass losses were very fast for TCNQG1 and TCNQG2. The DTG curve showed that the mass losses of functionalized graphene occurred in a few steps as shown in Fig. 6. Major losses of TCNQG1 and TCNQG2 occured at 766 and 740 °C, respectively. It may be attributed to the degradation of non-covalently adsorbed TCNQ to the surface of the graphene sheets. The onset degradation temperatures for TCNQG1 and TCNQG2 were 136 and 148 °C, respectively. Interestingly, the mass loss of TCNQG2 was very fast compared to that of TCNQG1. The enhanced thermal stability of TCNQG1 as compared to the TCNQG2 may be due to the less non-covalently adsorbed TCNQ and scanty amounts of oxygen functional groups in TCNQ1, which is consistent with the FT-IR and XPS observations. Mass losses of TCNQG1 and TCNQG2 at 800° C were 30% and 42%, respectively, confirming our earlier observations regarding the effects of TCNQ concentration on graphite exfoliation and surface modification of graphene.[9,23]

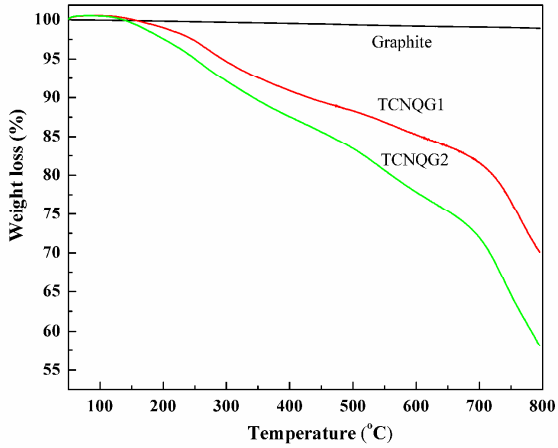

Fig. 6 TG and DTG curves of pure graphite, TCNQG1, and TCNQG2 confirming surface modification of graphene.

3.6 Electrochemical performance study

The electrochemical performances of TCNQG1 and TCNQG2 were measured in 1 M Na_2SO_4 and 1 M KOH solution as shown in Fig. 7-10. Fig. 7 shows the CV curves of TCNQG1 and TCNQG2 in both electrolytes at a scan rate of 20 mV s^{-1}. The CV curves of the functionalized graphene (TCNQG1 and TCNQG2) in Na_2SO_4 and KOH have a nearly rectangular shape, indicating good reversibility of ions at the interface of electrode and electrolyte.[39-42] This kind of CV curves indicated that the supercapacitor performance of the electrode materials arose due to the formation of electrical double layers at the electrode-electrolyte interface. The double layer formed due to the electrostatic interactions between the electrolyte and TCNQ-functionalized graphene sheets. In comparison to TCNQG2, the shape of the CV curves of TCNQG1 was more rectangular. However, the area covered by the CV curves of TCNQG2 was higher than that of TCNQG1 studied in the both electrolytes at a scan rate of 20 mV s^{-1}. Moreover, the CV curves of TCNQG2 are little distorted from rectangular shape as compared to the TCNQG1. These results indicate that the higher capacitive current is observed for TCNQG2 due to more polarization in presence of excess TCNQ-anion on the surface of exfoliated graphene sheets. In addition, the diffusion of ions in solution is relatively slower than electron transition. Therefore, the CV curves of TCNQG2 are distorted from the rectangular shape.[42] The presence of more TCNQ anions on the surface of TCNQG2 is supported by TGA, FT-IR and Raman spectroscopy analysis. Therefore, TCNQG2 had a better capacitive current as compared to the TCNQG1. In addition, oxygen moieties on the surface of graphene play a significant role in controlling the degree of polarization, double layer formation and electron transportation between the electrolyte and current collector.

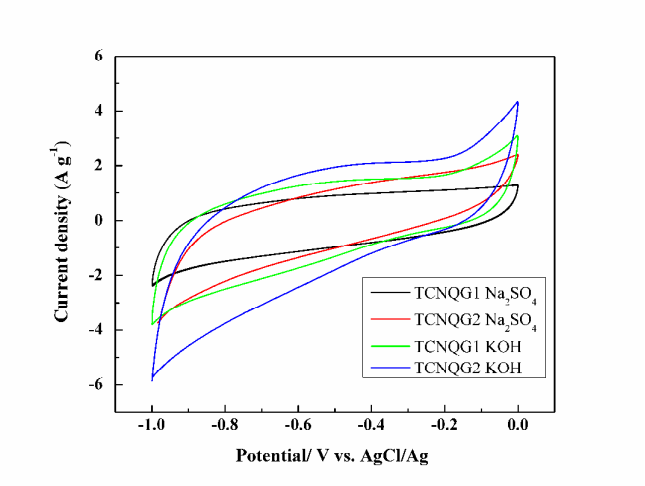

Fig. 7 Cyclic voltammetry graphs of TCNQG1 and TCNQG2 in 1 M Na_2SO_4 and 1 M KOH electrolyte at a scan rate of 20 mV s^{-1}.

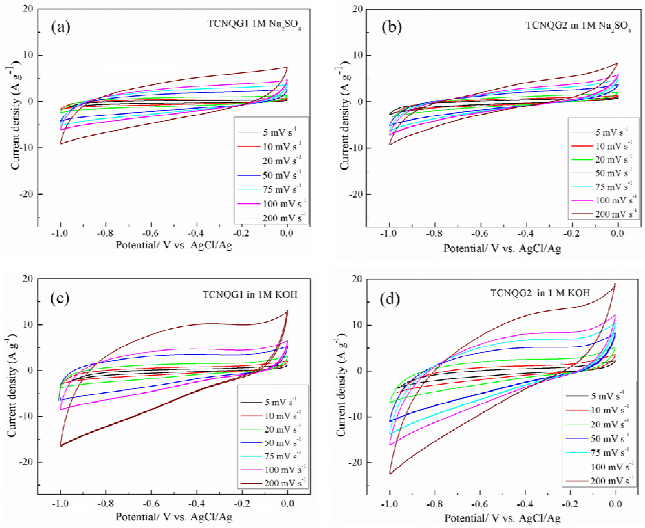

Fig. 8 Cyclic voltammetry performance of (a) TCNQG1 in 1 M Na_2SO_4, (b) TCNQG2 in 1 M Na_2SO_4, (c) TCNQG1 in 1 M KOH, and (d) TCNQG2 in 1 M KOH at different scan rates.

The areas covered by the CV curves of TCNQG1 and TCNQG2 are significantly higher when 1 M aqueous KOH solution was used as an electrolyte than 1 M Na_2SO_4 solution. The CV curves of TCNQG1 and TCNQG2 at different scan rates measured in both electrolytes (1 M KOH and 1 M Na_2SO_4) are shown in Fig. 8(a-d). The superior electrochemical performance in KOH electrolyte may be attributed to its better wettability with the electrode materials as compared to that of the Na_2SO_4 electrolyte. Moreover, an aqueous solution of KOH served a dual role as an electrolyte as well as a surface activating agent for graphene, as reported by Wang, et al.[43] In particular, the charge accumulation on the electrode materials depends on the electrode potential and surface functional groups. The presence of TCNQ-anion and oxygen functionality on the surface of graphene make it negatively charged. Therefore, it is expected that the electrical diffusion layer is formed at the electrode-electrolyte interfaces. However, the establishment of adsorption equilibrium is a very slow process and thus, it is formed at low scan rate. On the other hand, at high scan rate the shape of the CV curves is distorted from near rectangular shape due to the polarization.[42] At high scan rate, the electronic velocity of flow is faster than that of the ion transportation in solution leading to the downgrading of capacitive behavior of the electrode materials. It is interesting to note that at high scan rate an unexpected increase in current is recorded (near +0.0 V and –1.0 V) possibly due to the reaction of KOH with the active sites of the TCNQ functionalized graphene and decomposition of electrolyte as reported by Gu et al. for sulfur-containing activated carbon electrodes.[44] The nature of the CV curves studied in Na_2SO_4 electrolyte is markedly different with those of the CV curves studied in KOH electrolyte. It is seen that the shape of the CV curves remains unchanged in the Na_2SO_4 electrolyte even at high scan rate. It may be attributed to the high stability window of Na_2SO_4 electrolyte in neutral pH.[45]

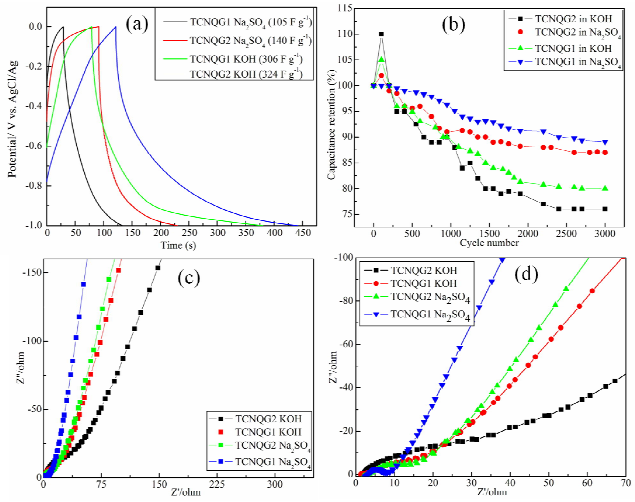

Fig. 9 (a) Charge discharge graphs of TCNQG1 and TCNQG2 in 1 M Na_2SO_4 and 1 M KOH at a current density of 1 A g^{-1}; (b) capacitance retention of TCNQG1 and TCNQG2 in 1 M Na_2SO_4 and 1 M KOH at a current density of 1 A g^{-1}; (c) EIS of TCNQG1 and TCNQG2 at an open circuit voltage of 1 M Na_2SO_4 and 1 M KOH; (d) EIS of TCNQG1 and TCNQG2 shown at high frequency region.

Galvanometric charge discharge was employed to estimate the specific capacitance of TCNQG1 and TCNQG2, as shown in Fig. 9(a). The specific capacitance was calculated using the equation C_{sp} = applied current × discharge time /(mass × operating voltage window). Charge-discharge experiments were carried out in the voltage range of 0.0 to -1.0 V at a constant current density of 1 A g^{-1}. The specific capacitances of TCNQG1 and TCNQG2 in KOH electrolyte were 324 and 306 F g^{-1}, respectively. The corresponding values in Na_2SO_4

electrolyte were 105 and 140 F g^{-1}, respectively. The galvanostatic charge-discharge graphs showed long discharge times, indicating that capacitance performance increased due to the higher polarization. The higher specific capacitance of TCNQG1 and TCNQG2 in KOH clearly indicated that the specific capacitance value was dependent on the penetration of electrolyte and surface polarization. The capacitance retention of TCNQG2 in Na_2SO_4 and KOH after 3000 cycles (at a current density of 1 A g^{-1}) was 87 and 76%, respectively (Fig. 9b). In contrast, the capacitance retention of TCNQG1 in Na_2SO_4 and KOH electrolyte after 3000 cycles was ~89 and 80%, respectively. The lower electrochemical cyclic stability of TCNQG2 than TCNQG1 is possibly due to the decomposition of adsorbed TCNQ on the surface of the graphene sheets. FT-IR spectra, deconvoluted XPS, and TGA showed that TCNQG2 contained a higher amount of surface modifiers than that of TCNQG1. These results suggest that high content of TCNQ o n the surface of graphene is good for high specific capacitance but with the loss of electrochemical stability. The electrochemical performance and sample preparation conditions of TCNQ functionalized graphene have been compared in Table S1 of supporting information. It shows that the capacitive performances of the TCNQ functionalized graphene sheets are better than that of the existing state-of-the-art compounds.

The IR drops of TCNQG2 and TCNQG1 in Na_2SO_4 solution are 0.16 and 0.08 V, respectively. The IR drops of TCNQG2 and TCNQG1 in KOH aqueous electrolyte are 0.09 and 0.07 V, respectively. In addition, the IR drop of surface-functionalized graphene sheets is higher in the KOH electrolyte than the Na_2SO_4 electrolyte. This may be due to weak interactions between electrode and Na_2SO_4 electrolyte, resulting in easy ions migration during discharge. Fig. 9(a) shows the existence of a large IR drop due to the internal resistance of the electrolyte to electrode. Note that the IR drop of TCNQG2 was higher than that of TCNQG1, likely due to the higher content of adsorbed TCNQ. AFM and TEM image analysis showed that the exfoliation of graphite was greater in the presence of a higher amount of TCNQ electrolyte than a lower amount, resulting in the formation of thinner graphene sheets. The thinner layers of TCNQG2 may have resulted in the generation of several random nano-porous channels and higher polarization that hindered the migration of ions during discharging.[46] All these factors explain the larger IR drop of TCNQG2 than that of TCNQG1. The IR drop of surface-functionalized graphene sheets was higher in the KOH electrolyte than the Na_2SO_4 electrolyte. This may be due to weaker interactions of Na_2SO_4 and cell components, making it too easy for ions to migrate during discharge.

The impedance spectroscopic measurements were carried out in both electrolytes at an open circuit voltage. Nyquist plots of TCNQG2 and TCNQG1 measured in both electrolytes are shown in Fig. 9(c). EIS (Z') represents the series resistance, which depends on electron transportation within the cell component. Z" is the complex part of resistance representing mass diffusion, and depends on layer structure, the porosity of the material, and concentration surface polarization. In an ideal capacitor, the Z' value should be very small and Z" should be parallel to the Y-axis.[39,47,48] The bulk resistance (R_b) of an electrode material can be determined from the starting point on the real axis. The R_b values for TCNQG1 in KOH and Na_2SO_4 are found to be 1.38 and 1.61 Ω, respectively. In contrast, the R_b values for TCNQG2 in KOH and Na_2SO_4 are 2.08 and 1.57, respectively. The charge transfer resistance (R_{ct}) can be determined from the diameter of semi-circle from the EIS spectra as shown in Fig. 9(d). The R_{ct} values of TCNQG1 in KOH and Na_2SO_4 are 11.22 and 3.52 Ω respectively. In contrast, the R_{ct} values of TCNQG2 in KOH and Na_2SO_4 electrolyte are 13.84 and 7.82 Ω, respectively. The sum of bulk resistance and charge transfer resistance is higher in KOH electrolyte than that in Na_2SO_4 due to high degree of polarization. Furthermore, the total resistance of TCNQG2 is higher than that of TCNQG1 due to high absorption of TCNQ- anion, resulting in higher polarization with both kind of electrolytes and decreased ion transportation with respect to electron transition in the circuit. This observation is in good agreement with the IR drop values determined from the galvanometric charge-discharge graphs. It is noted that at low frequency region, the EIS spectra of both samples are parallel to the Y-axis. However, the spectra of the sample studied in Na_2SO_4 electrolyte are comparatively more parallel to the Y-axis than those in KOH electrolyte. It may be due to the surface polarization and control mass diffusion in the porous structure of the electrode for the sample studied in Na_2SO_4 electrolyte. These results clearly indicate that the charge transfer process is affected by porosity, amount of polarization. Finally, it is seen that the R_{ct} value of TCNQG1 is lower than that of TCNQG2 resulting better electron transportation in TCNQG1 electrode as compared to that of the TCNQG2.

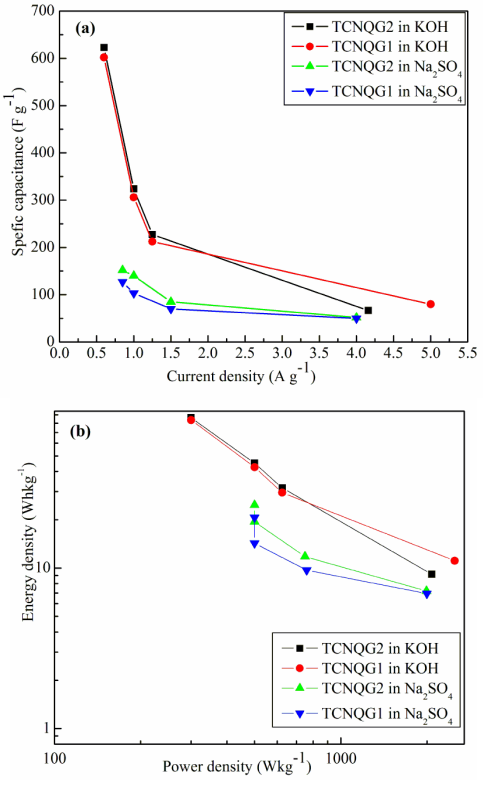

Fig. 10 (a) Specific capacitance vs. different current density; (b) specific energy density vs. specific power density (X and Y axis are shown in $\log_{10}$) of TCNQG1 and TCNQG2 in 1 M Na_2SO_4 and 1 M KOH.

Variations of specific capacitance with current density and corresponding energy density with power density are shown in Fig. 10 (a) and (b). As the current density increased, the capacitance value decreased, indicating that adsorption and absorption at high current density were not in equilibrium for either of the two electrolytes. Interestingly, the capacitance value of TCNQG1 at a high current density was higher than that of TCNQG2 in KOH. This indicates that TCNQG1 is thicker and has a lower degree of polarization than TCNQG2. Therefore, the TCNQG1 is capable to fast electron transition as well as ion diffusion at high current density. In contrast, specific capacitance decreased with increasing current density. So, at a high current density, the capacitances of TCNQG1 and TCNQG2 were nearly equal. Fig. 10 (b) shows the variation of power density according to energy density of TCNQG1 and TCNQG2. Energy density was calculated from the galvanometric charge-discharge curve at different current densities using the following equation:

Energy density = ½ × *specific capacitnce* × *(operating voltage window)*^{2}

Power density = *energy density/ discharge time*.

Specific energy density decreased with increasing power density for both TCNQG1 and TCNQG2, which is a common feature of energy storage devices.[47,49]

Energy density of TCNQG2 in KOH reached 86.9 Wh kg^{-1} at a power density of 300 W kg^{-1} and the energy density retention was 9.16 Wh kg^{-1} at a power density of 2079 W kg^{-1}. In contrast, the energy density of TCNQG1 was 83.66 Wh kg^{-1} when the power density was 300.27 W kg^{-1}, and energy density retention was 11.11 Wh kg^{-1} at a power density of 2499.75 W kg^{-1}. These results indicate that the energy density retention of TCNQG1 in KOH electrolyte was better than that of TCNQG2 in KOH electrolyte. However, the specific capacitance value of TCNQG2 was higher than that of TCNQG1. Therefore, the performance of an electrode in an energy storage device depends not only on the capacitance value, but also the electron transition and ion diffusion rates corresponding to the applied current density. In Na_2SO_4 electrolyte, the energy density and power density of TCNQG2 were 24.72 Wh kg^{-1} and 499.95 W kg^{-1}, respectively, and the energy density retention was 7.2 Wh kg^{-1} at a power density of 1993 W kg^{-1}. In contrast, the energy density and power density of TCNQG1 in Na_2SO_4 electrolyte were 20.66 Wh kg^{-1} and 500 W kg^{-1}, respectively. The retention in energy density was 6.94 Wh kg^{-1} at a power density of 1998 W kg^{-1}. The above results indicate that the observed energy density measured in the Na_2SO_4 electrolyte was lower than that measured in the KOH electrolyte. However, the power density measured in the Na_2SO_4 electrolyte was comparatively higher than that measured in the KOH electrolyte. The above results indicated that energy density in KOH increased due to high capacitance value. The capacitance behavior depended on the degree of polarization and ions transportation.

Conclusions

TCNQ-functionalized water dispersible graphene through one-step electrochemical exfoliation were prepared successfully. We characterized the functionalized graphene by FT-IR, Raman, and XPS analysiss of these data provided clear evidence of non-covalent functionalization by TCNQ. AFM image analysis confirmed that the concentration of TCNQ anions as electrolytes played an important role in the exfoliation of graphite. The average thickness of graphene sheets was 1.0 nm when a high concentration of TCNQ was used (TCNQG2) and 2.5 nm when a low concentration of TCNQ was used (TCNQG1). TEM and HR-TEM images also indicated the formation of few-layer graphene due to electrochemical exfoliation of graphite. This technique to prepare functionalized graphene is cost-effective, green, and simple. In addition, the process is very easy to scale-up for further applications. The electrochemical performances of TCNQ-functionalized electrodes were evaluated in terms of CV, galvanometric charge-discharge characteristics, and EIS. It has been found that specific capacitance depended not only on the concentration of TCNQ used as electrolyte and surface modifier, but was also dependent on the type of electrolyte used in the electrochemical performance study. The highest specific capacitance was 324 F g^{-1} at a current density of 1 A g^{-1} in 1 M KOH electrolyte (TCNQG2). Electrochemical performance analysis confirmed that high specific capacitance was due to the formation of double layers via penetration of electrolyte. The high specific capacitance of TCNQ-functionalized graphene indicates that this material can be used as a next-generation electrode material for green energy storage devices.

Acknowledgements

This study was supported by the Converging Research Center Program (2013K000404) through the Ministry of Science, ICT & Future Planning and the Basic Science Research Program (NRF-2013R1A1A2011608) and the BK Plus Global Program through the National Research Foundation (NRF) funded by the Ministry of Education of Korea.

Notes and references

[a] *Advanced Materials Research Institute for BIN Fusion Technology & Department of BIN Fusion Technology, Chonbuk National University, Jeonju, Jeonbuk, 561-756, Republic of Korea, Fax:+82 63 270 2341; Tel: +82 63 270 2342.*

[b] *Surface Engineering & Tribology Division, Council of Scientific & Industrial Research -Central Mechanical Engineering Research Institute, Mahatma Gandhi Avenue, Durgapur -713209, India Fax: +91-343-2548204; Tel: +919647205077.*

[c] *Advanced Wind Power System Research Center, Chonbuk National University, Jeonju, Jeonbuk, 561-756,Republic of Korea, Fax:+82 63 270 2341; Tel: +82 63 270 2342.*

[*] *Correspondence to: Prof Joong Hee Lee(jhl@jbnu.ac.kr) and Dr. Nam Hoon Kim (namhk99@naver.com)*

Electronic Supplementary Information (ESI) available: Schematic diagram of electrochemical exfoliation mechanism, XPS survey spectra

of pure graphite, TCNQG1 and TCNQG2, deconvoluted C1s spectra of grapgite and comparison of materials preparation and electrochemical performance of TCNQ functionalized graphene sheets with the existing state-of-the-art compounds. See DOI: 10.1039/b000000x/

1 K. S. Novoselov, A. K. Geim, S. V. Morozov, D. Jiang, Y. Zhang, S. V. Dubonos, I. V. Grigorieva and A. A. Firsov, *Science*, 2004, **306**, 666-669.
2 C. Berger, Z. M. Song, X. B. Li, X.S. Wu, N. Brown, C. Naud, D. Mayo, T. B. Li, J. Hass, A. N. Marchenkov, E.H. Conrad, P. N. First and W. A. de Heer, *Science*, 2006, **312**, 1191-1196.
3 A. K. Geim and K. S. Novoselov, *Nat. Mater.*, 2007, **6**, 183 - 191.
4 S. Stankovich, D. A. Dikin, G. H. B. Dommett, K. M. Kohlhaas, E. J. Zimney, E. A. Stach, R. D. Piner, S. T. Nguyen and R. S. Ruoff, *Nature*, 2006, **442**, 282-286.
5 H. Chen, M. B. Müller, K. J. Gilmore, G. G. Wallace and D. Li, *Adv. Mater.*, 2008, **20**, 3557-3561.
6 M. Kalbacova, A. Broz, J. Kong and M. Kalbac, *Carbon*, 2010, **48**, 4323-4329.
7 Z. Lin, Y. Liu, Y. Yao, O. J. Hildreth, Z. Li, K. Moon and C. Wong, *J. Phys. Chem. C*, 2011, **115**, 7120-7125.
8 H. Liu, J. Gao, M. Xue, N. Zhu, M. Zhang and T. Cao, *Langmuir*, 2009, **25**, 12006-12010.
9 T. Kuila, A. K. Mishra, P. Khanra, N. H. Kim, M. E. Uddin and J. H. Lee. *Langmuir*, 2012, **28**, 9825-9833.
10 M. A. Rafiee, J. Rafiee, I. Srivastava, Z. Wang, H. Song, Z. Z. Yu and N. Koratkar, *Small*, 2009, **6**, 179-183.
11 T. Kuila, S. Bose, P. Khanra, N. H. Kim, K. Y. Rhee and J. H. Lee, *Compos. Part A-Appl. Sci.*, 2011, **42**, 1856-1861.
12 Y. Ohno, K. Maehashi, Y. Yamashiro and K. Matsumoto, *Nano. Lett.*, 2009, **9**, 3318-3322.
13 T. Chen , W. Hu , J. Song , G. H. Guai and C. M. Li, *Adv. Funct. Mater.*, 2012, **22**, 5245-5250.
14 D.W. Zhang, X. D. Li, H.B. Li, S. Chen, Z. Sun, X. J. Yin, and S. M. Huang, *Carbon*, 2011, **49**, 5382-5388.
15 D. Du, Z. Zou, Y. Shin, J. Wang, H. Wu, M. H. Engelhard, J. Liu, I. A. Aksay and Y. Lin, *Anal. Chem.*, 2010, **82**, 2989-2995.
16 H. Xu and K. S. Suslick, *J. Am. Chem. Soc.*, 2011, **133**, 9148-9151.
17 N. Liu, F. Luo, H. Wu, Y. Liu and C. Zhang, *J. Chen. Adv. Funct. Mater.*, 2008, **18**, 1518-1525.
18 J. Wang, K. K. Manga, Q. Bao and K. P. Loh, *J. Am. Chem. Soc.*, 2011, **133**, 8888-8891.
19 R. Hao, W. Qian, L. Zhang and Y. Hou, *Chem. Commun.*, 2008, **45**, 6576-6578.
20 L. Ren, L. Fu, Y. Liu, S. Chen and Z. Liu, *Adv. Mater.*, 2009, **21**, 4742-4746.
21 A. C. Ferrari, J. C. Meyer, V. Scardaci, C. Casiraghi, M. Lazzeri, F. Mauri, S. Piscanec, D. Jiang, K. S. Novoselov, S. Roth and A. K. Geim, *Phys. Rev. Lett.*, **2006**, 97, 187401.
22 H. Hermandez, V. Nicolosi, M. Lotya, F. M. Blighe, Z. Sun, S. De, I. T. McGovern, B. Holland, M. Byrne, Y. K. Gun'Ko, J. J. Boland, P. Niraj, G. Duesberg, S. Krishnamurthy, R. Goodhue, J. Hutchison, V. Scardaci, A. C. Ferrari and J. A. Coleman, *Nat. Nanotechnol.*, **2008**, 3, 563-568.
23 S. S. Li, K. H. Tu, C. H. Lin, C. W. Chen and M. Chhowalla. *ACS Nano*, **2010**, 4, 3169-3174.
24 A. Schlierf, H. Yang, E. Gebremedhn, E. Treossi, L. Ortolani, L. Chen, A. Minoia, V. Morandi, P. Samorì, C. Casiraghi, D. Beljonne and V. Palermo, *Nanoscale*, **2013**, 5, 4205-4216.
25 H. L. Guo, X. F. Wang, Q. Y. Qian, F. B. Wang and X. H. Xia. *ACS. Nano.*, 2009, **3**, 2653-2659.
26 D. Chen, L. Li and L. Guo, *Nanotechnology*, 2011, **22**, 325601.
27 K. Yase, O. Okumura, T. Kobayashi and N. Uyeda, *Bull. Inst. Chem. Res.*, 1984, 62, 242-250.
28 T. A. Pham, J. S. Kim, J. S. Kim and *Y. T. Jeong*, Colloid. Surface. A, 2011, 384, 543-548.
29 P. Khanra, T. Kuila, N. H. Kim, S. H. Bae, D. Yu and J. H. Lee, *Chem. Eng. J.*, 2012, **183**, 526-533.
30 S. Piscanec, M. Lazzeri, J. Robertson, A. C. Ferrari and F. Mauri, *Phys. Rev. B*, 2007, **75**, 35427.
31 M. Lazzeri, S. Piscanec, F. Mauri, A. C. Ferrari and J. Robertson, *Phys. Rev. B*, 2006, **73**, 155426.
32 R. Voggu, B. Das, C. S. Rout and C. N. R. Rao, *J. Phys.: Condens. Matter.*, 2008, **20**, 472204.
33 A. C. Ferrari, *Solid State Commun.*, 2007, **143**, 47-57.
34 Y. Y. Wang, Z. H. Ni, T. Yu, Z. X. Shen, H. M. Wang, Y. H. Wu, W. Chen and A. T. S. Wee, *J. Phys. Chem. C*, 2008, **112**, 10637-10640.
35 X. Fan, W. Peng, Y. Li, X. Li, S. Wang, G. Zhang and F. Zhang, *Adv. Mater.*, 2008, **20**, 4490-4493.
36 P. Khanra, T. Kuila, S. H. Bae, N. H. Kim and J. H. Lee, *J. Mater. Chem.*, 2012, **22**, 24403.
37 K. J. Boyd, D. Marton, S. S. Todorov, A. H. Al-Bayati, J. Kulik, R. A. Zuhr and J. W. Rabalais, *J. Vac. Sci. Technol. A.*, 1995, **13**, 2110-2122.
38 X. Xia, Q. Hao, W. Lei, W. Wang, H. Wang and X. Wang, *J. Mater. Chem.*, 2012, **22**, 8314-8320.
39 B. E. Conway, Kluwer Academic/Plenum Publishers: New York, 1999.
40 E. Frackowiak and F. Beguin, *Carbon*, 2001, **39**, 937-950.
41 W. Gu, M. Sevilla, A. Magasinski, A. B. Fuertes and G. Yushin, *Energ. Environ. Sci.*, 2013, **6**, 2465-2476.
42 D. Antiohos, K. Pingmuang, M. S. Romano, S. Beirne, T. Romeo, P. Aitchison, A. Minett, G. Wallace, S. Phanichphant and J. Chen, *Electrochim. Acta*, 2013, **101**, 99-108.
43 Y. Wang, Z. Shi, Y. Huang, Y. Ma, C. Wang, M. Chen and Y. Chen, *J. Phys. Chem. C*, 2009, **113**, 13103-13107.
44 W. Gu, M. Sevilla, A. Magasinski, A. B. Fuertes and G. Yushin, *Energ. Environ. Sci.*, 2013, **6**, 2465-2476.
45 L. Demarconnay, E. Raymundo-Piñero and F. Béguin, *Electrochem. Commun.*, 2010, **12**, 1275-1278.
46 D. W. Wang, F. Li, H. T. Fang, M. Liu, G. Q. Lu and H. M. Cheng, *J. Phys. Chem. B*, 2006, **110**, 8570-8575.
47 C. Liu, Z. Yu, D. Neff, A. Zhamu and B. Z. Jang, *Nano Lett.*, 2010, **10**, 4863-4868.
48 B. Wang, D. Guan, Z. Gao, J. Wang, Z. Li, W. Yang and L. Liu, *Mater. Chem. Phys.*, 2013, **141**, 1-8.

49 T. Christen and M. W. Carlen, *J. Power Sources*, 2000, **91**, 210-216.

Table of Contents